

# Thin layers of microwave absorbing metamaterials with carbon fibers and FeSi alloy ribbons to enhance the absorption properties

Lingxi Huang, Yuping Duan\*, and Huifang Pang

Key Laboratory of Solidification Control and Digital Preparation Technology (Liaoning Province), School of Materials Science and Engineering, Dalian University of Technology, Dalian 116085, P.R. China

Received: 25 October 2022 / Accepted: 23 November 2022

**Abstract.** In order to break through the bottleneck of narrow effective absorption bandwidth (reflection loss  $RL \leq -10$  dB) of microwave absorbing materials, herein, we fabricate the metamaterials with carbon fiber (CF) and FeSi alloy (FSA) ribbon metastructure which is distributed in the carbonyl iron powders (CIP)/polyurethane (PU) matrix. The experimental results show that the microwave absorption capacity of the matrix can be significantly enhanced by CF. Compared with the pure matrix, the effective absorption bandwidth increases from 9.4–13.44 GHz to 11–16.8 GHz when the CF is parallel to the electric field vector and the spacing between adjacent CF is 20 mm. Furthermore, the CF and FSA ribbons are arranged in the matrix as an orthogonal arrangement, and the best absorption bandwidth cover 9.76–14.46 GHz when the electric field is parallel and 9.96–14.1GHz when the electric field is vertical when the spacing is 30 mm. The electromagnetic simulation of the metamaterials is calculated, it is proved that the increase of effective absorption bandwidth is due to the strengthening of carbon fiber and its coupling with FSA ribbon. This paper provides a new research path for improving the absorption properties of thin layer microwave absorbing materials.

**Keywords:** Microwave absorption materials / metamaterials / carbon fibers / FSA ribbons / carbonyl iron

## 1 Introduction

The broad-bandwidth and strong absorbers of microwave have applications in satellite communications [1,2], stealth [3], eliminating electromagnetic pollutions [4], etc. A lot of microwave absorbing material were developed to achieve broadband absorption by researchers [5], the absorbers according to the mechanism of loss can be classified as dielectric loss and magnetic loss material [6–8], the dielectric loss of materials including graphene [9–11], carbon nanotubes [12,13], carbon fiber [14], manganese dioxide [15], etc., magnetic loss materials mainly include carbonyl iron [16,17], ferrite [18], iron alloy [19], high entropy alloys [20] and so on. Most of the previous studies combined these two types of materials to improve impedance matching and achieve broadband absorption. For example, Che et al., fabricated multishell  $TiO_2@Fe_3O_4@$ polypyrrole(PPy) heterojunction core-shell structure materials, the maximum reflection loss (RL) can reach  $-61.8$  dB with a thickness of 3.2 mm, the effective absorption bandwidth cover 6.0 GHz under 2.2 mm thickness [21]. Ning and coworkers prepared the Co@C/MXene composite with different dimension, the maximum

effective absorption bandwidth of absorber can reach 5.8 GHz under 2.0 mm, and the best absorption peak could reach  $-50.5$  dB [22]. Liu and coworkers fabricated the metal-organic frameworks (MOFs) made up of Co@N-doped carbon nanocages via synergistic protecting-etching strategy, the effective absorption bandwidth covered 5.1 GHz under 1.9 mm and the best RL value was reached  $-60.6$  dB at 2.4 mm [23]. However, it is difficult to realize broadband absorption by only relying on the intrinsic properties of materials. In this context, the effective absorption bandwidth can be further improved by introducing metastructure to the materials [24].

Therefore, numerous researchers fabricate microwave absorbing materials into a variety of metastructures [25], resulting in multiple coupling effects between materials and metastructures to continue to improve the effective absorption bandwidth. Previous studies have been demonstrated that the shape and arrangement form of the unit cells have a great influence on the absorption performance [26], such as Zhang et al. proposed metamaterial absorbers made of windmill-shaped unit cells to realize broad band absorption, the unit cell was made up of indium tin oxide (ITO) film, the effective absorption bandwidth range from 8.3 to 17.4 GHz under 3.85 mm thickness, and the metamaterial was also optically transparent [27]. The metamaterials with square unit cells that made up of

\* e-mail: [duanyyp@dlut.edu.cn](mailto:duanyyp@dlut.edu.cn)

polypropylene nonwoven fabrics and reduced graphene oxide were fabricated by Song and coworkers, the metamaterials achieved ultrabroad band effective absorption that from 2 to 18 GHz under approximate 12 mm thickness, and the absorption property also could be manipulated by weather [28]. Li and Guan and other scholars processed ITO (indium tin oxide) into ring elements and arranged it in an upright sequence, which could make the ring ITO form vortex current to attenuate the magnetic field, so that ITO, which is an electrically losing material, also possessed magnetic resonance properties. Effective absorption bandwidths with absorption rates greater than 85% cover 5.5–19.7 GHz and 22.5–27.5 GHz under 5.5 mm thickness [29]. Furthermore, the metastructure with shape of grating [30], pyramid [31] and so on also could improve the absorption performance. Our previous works also demonstrated that the bionic metastructures also could improve the absorption property [32–34]. However, the previous microwave absorbing metamaterials still have to be relatively large thickness to achieve broadband absorption [28]. Until now, the broadband absorption of highly thin absorbing material has been particularly difficult due to the deep subwavelength constraints of the absorber thickness. The absorption bandwidth constrained by absorber thickness could be illustrated by Rozanov limit [35]:

$$\frac{\Delta\lambda}{d} < \frac{16\mu_s}{|\ln\rho_0|}, \quad (1)$$

where  $\Delta\lambda$  is operating bandwidth,  $d$  and  $\mu_s$  are thickness and static permeability of the slab material respectively, and  $\rho_0$  is reflection coefficient. It can be found that the maximum bandwidth is restricted by  $\mu_s$  and  $d$ .

In this context, in this paper, a new type of metamaterial is presented. The metastructure is composed of metastructure sandwiched between two layers of absorbing matrix. Specifically, we demonstrate a broadband and enhanced absorption metamaterial in microwave band with carbon fibers (CF) grating and FeSi alloy (FSA) ribbons in carbonyl iron powder (CIP)/polyurethane (PU) matrix of deep subwavelength thickness (1 mm), CF has excellent dielectric loss and conductance loss ability, and FSA ribbons have decent magnetic loss performance. The combination of these two materials facilitates excellent absorption performance, thus the mentioned two materials were achieved as absorbers to construct metamaterials in this paper, and corresponding mechanism of materials and metastructures coupling is explored.

## 2 Experimental details

### 2.1 Preparation of metamaterials

The PU (Shanghai Hecheng Polymer Technology Co., Ltd., China) and CIP (Shanxi Xinghua Chemical Co., Ltd., China) were used to fabricate microwave absorption matrix, the mass ratio of above mentioned two materials was 4:1. The mixture of matrix was stirred with rotate speed of 500 rpm and ultrasonic oscillation for 15 min, respectively, then these steps were repeated. The suspension was coated on a square

aluminum substrate with dimension of 200 mm × 200 mm × 1.5 mm, and the suspension as bottom matrix with 0.5 mm thickness. The CF (AKSA, turkey) and FSA ribbons were paved on the bottom matrix by orthogonal arrangement, then the half-finished metamaterials was solidified at 25 °C for 12 h. Then the top matrix was coated on the half-finished metamaterials as above mentioned step. The resulting samples contained CF and FSA ribbons with thickness of 1 mm was obtained, and this paper generated a pure matrix sample for reference. The preparation technology of FSA ribbons could be found in our previous study.

### 2.2 Characterization of metamaterials and corresponding matters

The scanning electron microscopy (SEM, Zeiss, Supra 55) was used to measure the morphology of the materials. The Agilent 85050D vector network analyzer was carried out the complex permittivity and permeability over a frequency range of 8–18 GHz, which samples were molded to form a cylindrical toroidal specimen with an outer diameter of 7.0 mm and an inner diameter of 3.04 mm. The RL of the metamaterials was measured by a HP8720B Vector Network Analyzer using the arch method, and the incident angle was 10°. The conductivity of materials was measured by the RTS-9 4-point probe resistivity measurements system.

### 2.3 The simulation models

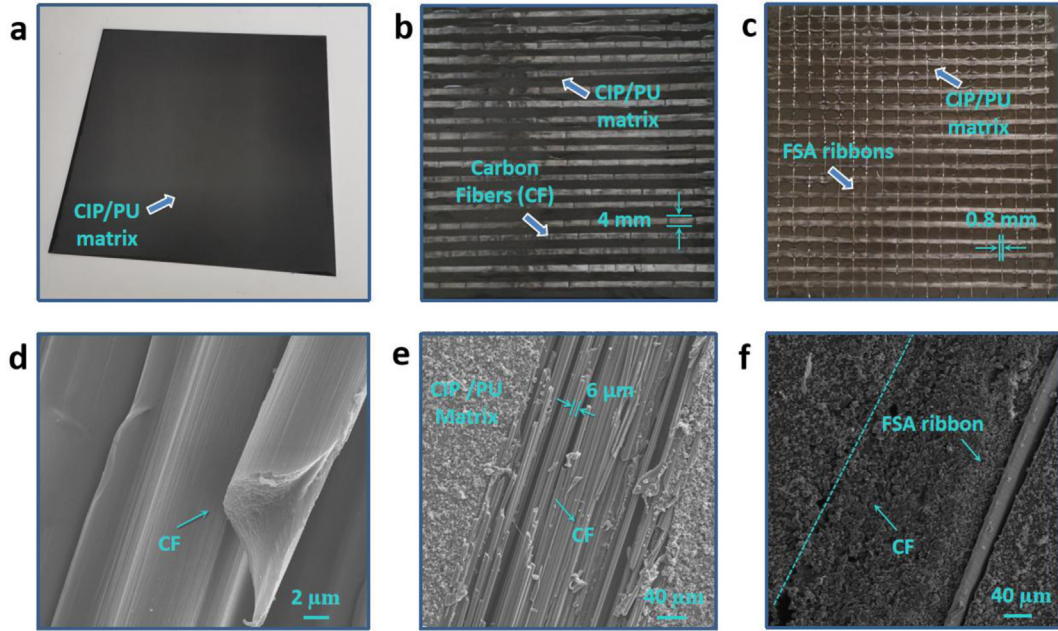
Corresponding model construction condition and method could be found in our previous studies [3], the parameters (relative permittivity = 78.41, relative permeability = 0.59, dielectric loss tangent ( $\tan\delta_\epsilon$ ) = 3.41, magnetic loss tangent ( $\tan\delta_\mu$ ) = 0.59, and conductivity of 464.9 S/m) of specimen were input into the model.

## 3 Results

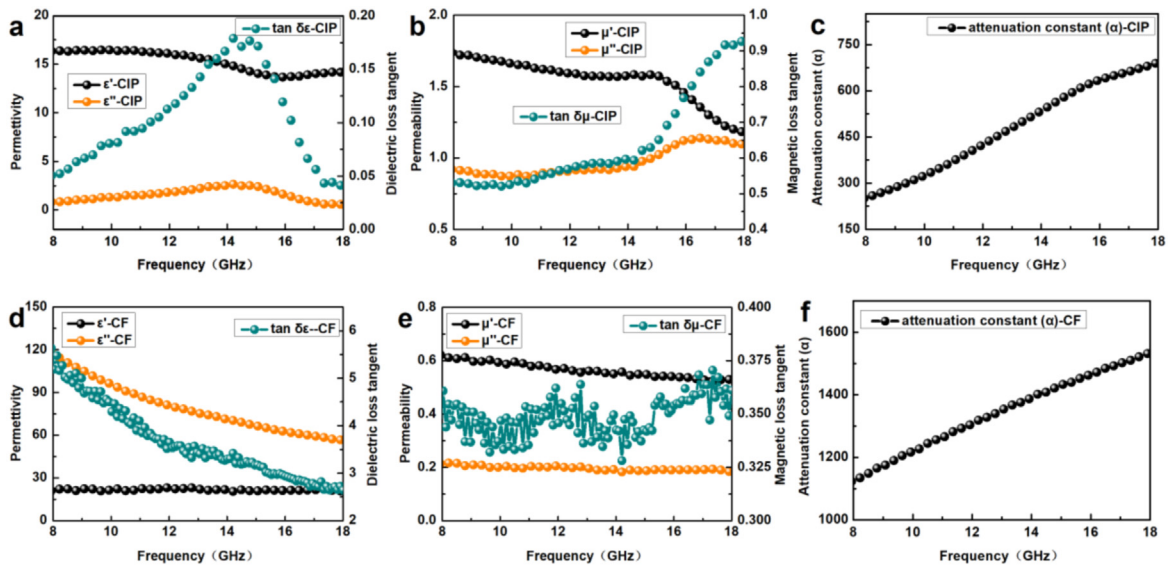
### 3.1 Material characterizations

Figure 1a shows the appearance of the sample, the size of the sample is 200 \* 200 mm and the thickness is 1 mm. This material with a interior sandwich structure, the upper and lower layers are matrix materials mixed with carbonyl iron and polyurethane resin at a mass ratio of 4:1, and the metastructure composed of CF and FSA ribbons sandwiched in the middle. It can be seen from Figure 1b that the CF is parallel arranged in the material, and the CF and FSA ribbons are distributed in an orthogonal way (Fig. 1c). The distribution of CIP, CF and FSA in the material is shown in Figures 1d–1f. CF with diameter of 6 μm, which is uniformly distributed (Figs. 1d and 1e). The CF bundle consists of numerous single fibers (Fig. 1e) sandwiched in two layers of CIP/PU composites. The FSA ribbons are orthogonal to the CF, and both materials are sandwiched in a two-layer CIP/PU matrix (Fig. 1f).

Figures 2a, 2b show the electromagnetic parameters of CIP/PU matrix in the frequency range of 8–18 GHz, which shows that this matrix is a material with both dielectric and magnetic losses ability [36,37]. The real part of its complex permittivity ( $\epsilon_r = \epsilon' - \epsilon''$ ) is between 13 and 17, the



**Fig. 1.** (a) Photograph of the appearance of the microwave-absorbing metamaterial prepared in this paper; Photograph of metastructure distribution of (b) CF and (c) FSA ribbons; (d) SEM image of CF; (e) Cross-section morphology of sandwich structure formed by CF sandwiched in CIP/PU matrix; (f) Cross-section morphology of sandwich structure formed by CF and FSA ribbon sandwiched in CIP/PU matrix.



**Fig. 2.** (a) Permittivity and corresponding loss angle tangent, (b) Permeability and corresponding loss angle tangent, (c) Attenuation constant of CIP/PU matrix. (d) Permittivity and corresponding loss Angle tangent, (e) Permeability and corresponding loss Angle tangent, (f) Attenuation constant of CF.

maximum value is 16.47 (9.93 GHz), and the imaginary part is between 0.5 and 2.7. The maximum value is 2.65 (14.2 GHz). The ratio of the real part to the imaginary part of the permittivity is the tangent of the dielectric loss angle ( $\tan \delta_e = \epsilon''/\epsilon'$ ), which can represent the dielectric loss ability of the material. Figure 2a shows that the maximum

tangent of the dielectric loss angle is 0.18 (14.395 GHz). Similarly, the complex permeability of this material ( $\mu_r = \mu' - \mu''$ ) also shows that it has excellent magnetic loss characteristic, and the maximum real, imaginary, and loss angle tangent of the permeability are 1.73 (8.03 GHz), 1.13 (16.865 GHz), and 0.93 (17.91 GHz), respectively.

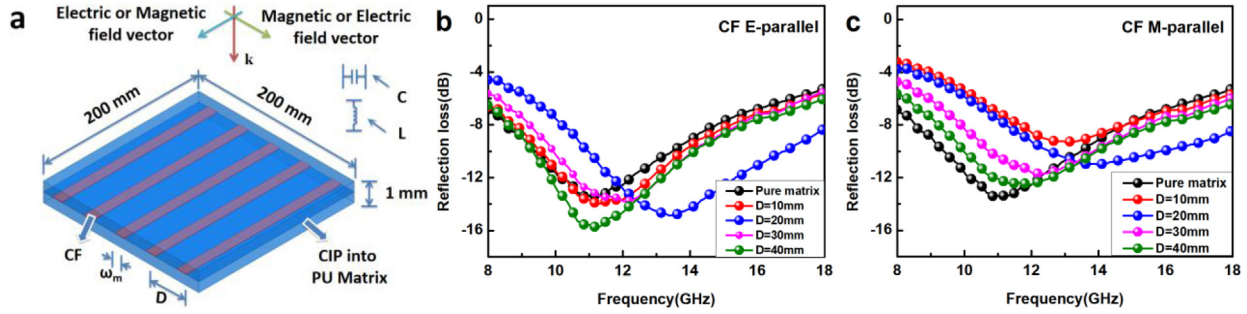


**Fig. 3.** (a) Schematic diagram of sandwich structure metamaterial containing parallel arranged CF, where  $D$  is the spacing between adjacent CF,  $\omega_m$  is the width of CF, and the thickness of CIP/PU resin matrix material above and below the CF is 0.5 mm,  $L$  and  $C$  represent the equivalent inductance and equivalent capacitance, respectively. RL of metamaterials of different spacing when CF (b) Parallel and (c) Perpendicular to incident electric field, respectively; the E-parallel and M-parallel represent the direction parallel to electric field vector and magnetic field vector, respectively.

Based on the joint action of dielectric loss and magnetic loss, these matrixes have a strong attenuation ability of microwave. It is represented by its attenuation constant ( $\alpha$ ) [38]:

$$\alpha = \frac{\sqrt{2}\pi f}{c} \sqrt{(\mu''\epsilon'' - \mu'\epsilon') + \sqrt{(\mu''\epsilon'' - \mu'\epsilon')^2 + (\mu''\epsilon'' + \mu'\epsilon')^2}} \quad (2)$$

where  $c$  is the light velocity,  $f$  is the frequency of microwave. The larger the value of attenuation constant  $\alpha$  is, the stronger the attenuation ability of the material to microwave is. Figure 2c shows that the matrix material exhibits excellent attenuation ability, and its value is proportional to the frequency, with a maximum attenuation ability of 689.24 (17.91 GHz). In contrast, the dielectric loss ability of CF is considerably stronger than that of CIP/PU matrix, with the imaginary part of permittivity up to 116.92 (8.03 GHz) and the corresponding loss angle tangent of 5.19. However, it can be seen from Figure 2e that the magnetic loss ability of CF is relatively weak. Therefore, although it has a stronger attenuation constant than the matrix, up to 1531.95 (17.91 GHz), the impedance mismatch is easy to be caused by the large difference between the permittivity and permeability, and it is not suitable to be used as a single microwave absorbing material matrix. Therefore, it is reasonable to distribute it in the matrix as a material to enhance absorption. Besides, the information on the electromagnetic parameters of FSA ribbons can be found in our previous papers [19]. In addition, conductance loss also plays an important role in the process of microwave absorption. Both CF and FSA ribbons are conductive materials, which contain a large amount of free charges. Under the action of electromagnetic field, these free charges form positive and negative charge accumulation at the interface, which consumes electromagnetic wave in the form of dipole polarization; the eddy current is also formed in the magnetic field, which consumes magnetic field by eddy current loss. More importantly, in the process of generating an electric current, electromagnetic waves are lost in the form of joule heat, which is an important reason why these two materials lose electromagnetic waves.

### 3.2 Absorption performance of metamaterials with different CF direction

When CF are parallel arranged in the matrix, the sandwiched metamaterial can exhibit directional microwave absorption. As shown in Figure 3a, according to the symmetry, the CF can exhibit two orientations with the electric field vector of the microwave: parallel and perpendicular to the electric field vector. When the CF is parallel to the electric field vector, it shows obvious improvement in both effective absorption bandwidth and absorption peak. As shown in Figure 3b, the effective absorption bandwidth of pure CIP/PU matrix without CF is 9.4–13.44 GHz, and the absorption peak is 13.40 dB (11.24 GHz). When CF is added and the spacing is 20 mm, the effective absorption bandwidth is 11–16.8 GHz, and the absorption peak is 14.86 dB (13.88 GHz). However, when the CF is perpendicular to the electric field vector, the absorption performance decreases (Fig. 3c). The main reason is that the role of the orientation of the two kinds of CF is different, this can be explained by equivalent circuit model, when the CF is parallel to the electric field, the free charge can move along the long distance thus equivalent inductance ( $L$ ), and when the CF perpendicular to the electric field vector, the energy of the oscillating electric field causes the accumulation of positive and negative charges on the side of the CF, so it is equivalent to capacitance ( $C$ ). Inductance and capacitance produce inductive reactance ( $X_L$ ) and capacitive reactance ( $X_C$ ), respectively, which have different characteristics:

$$X_C = \frac{1}{2\pi f C} \quad (3)$$

$$X_L = 2\pi f L \quad (4)$$

where  $f$  is the frequency of incoming microwaves. The shift of inductive reactance and capacitive reactance results in the shift of the overall impedance of the material, so the absorbing properties are also different. At the same time, we can see that the resonant frequency ( $f_0$ ) of metamaterial has also changed after the addition of CF, which commonly presents the characteristics of moving to high frequency.

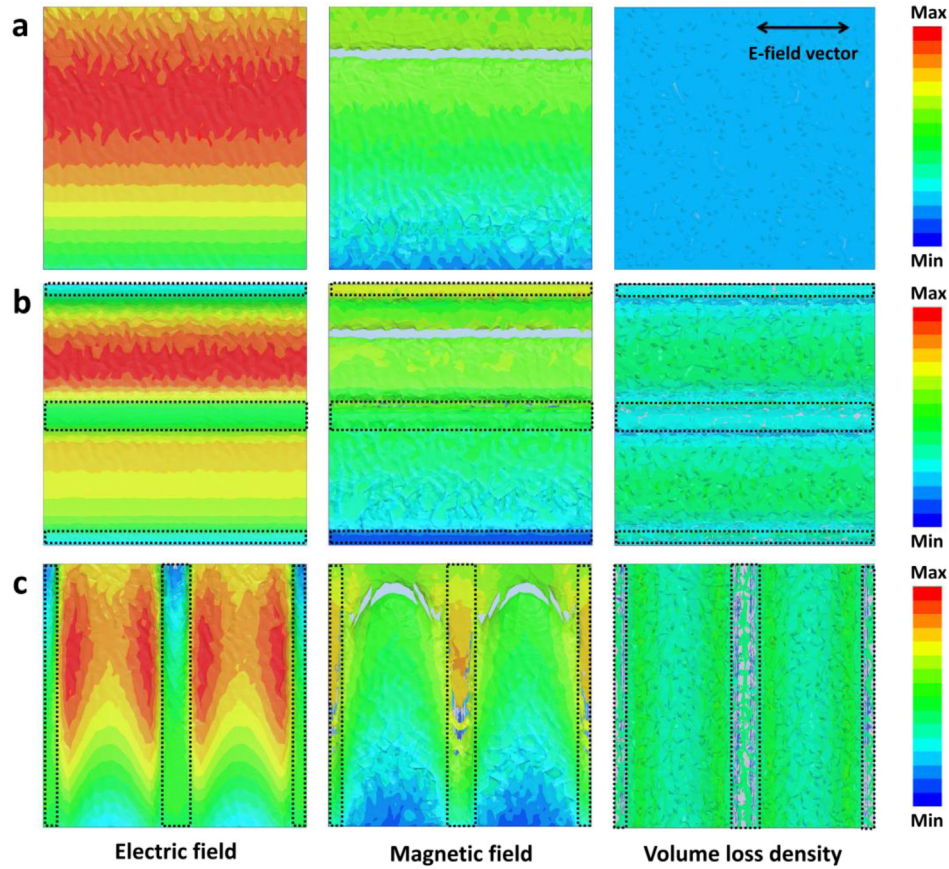


**Fig. 4.** Electric field, magnetic field and loss density distributions of (a) Pure CIP/PU matrix, (b) Sandwich metamaterial with CF parallel to electric field and (c) Sandwich metamaterial with CF perpendicular to electric field.

The characteristic is expressed as [19]:

$$f_0 = \frac{1}{2\pi\sqrt{LC}}. \quad (5)$$

It can be seen that the shift of inductance and capacitance caused by these two orientations will also affect the position of the resonant peak.

In order to further clarify the mechanism of absorbing effect of CF in the metamaterial, present works simulate and calculate the distribution of electromagnetic field and loss density in the material, as shown in Figure 4. The arrow direction in the upper right corner of the figure represents the direction of electric field oscillation. Figure 4a shows the distribution of electromagnetic field and loss density of pure CIP/PU matrix. It can be seen that without CF, the distribution of electromagnetic field intensity gradually changes from top to bottom, and part of the magnetic field intensity is blank. The main reason is that the incident angle is ten degrees instead of perpendicular incidence, resulting in a phase difference. In this case, the loss density is not high. When CF is added (the dotted line represents the edge of CF in the figure), the electromagnetic field distribution of the material when CF is parallel and perpendicular to the electric field vector is shown in Figures 4b and 4c respectively. When CF is

parallel to the electric field vector, the electric field distribution shows an interesting trend: The electric field strength of the middle CF is lower than of the pure matrix, while the CF on both sides has the opposite trend, the electric field strength of the CF on the top is lower than that of the pure matrix, but the CF on the bottom is increased. The trend of the magnetic field intensity is opposite, with the strength of the upper CF increasing and the strength of the lower CF decreasing. In other words, the distribution of the electric and magnetic field intensity is opposite locally through the regulation of CF, rather than the uniform distribution without CF. In this case, it is inevitable that CF makes the microwave appear abnormal mutation in the local phase, which is commonly caused by resonance, and also produces phase difference loss microwave. Besides, the loss density of the sample with CF parallel to the electric field is higher than that of the sample without CF.

When the CF is perpendicular to the electric field, another influence trend appears (Fig. 4c). The CF cuts the originally continuously distributed electric field into discontinuous parts, and connects the discontinuous parts of the magnetic field. The intensity distributions of the electric and magnetic fields are opposite, there is also an abnormal mutation in the phase of the electromagnetic field, so the corresponding resonance can also enhance the

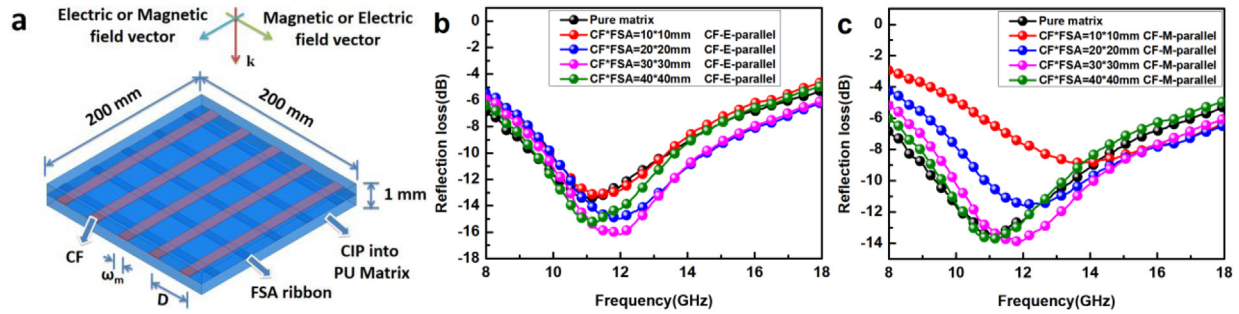


**Fig. 5.** (a) The schematic diagram of metamaterials with metastructure of CF and FSA ribbon are orthogonal arranged and sandwiched in CIP/PU matrix. RL of CF (b) Parallel to the electric field and (c) Perpendicular to the electric field at different spacing, the E-parallel and M-parallel represent the direction parallel to electric field vector and magnetic field vector, respectively.

absorption, which is demonstrated by the comparison of the distribution of the loss density. According to Figure 3c, however, RL performance is poor when the CF perpendicular to the electric, although the orientation of the CF can enhance the capacity of loss, but it can lead to variation of impedance matching, that generates metastructure on microwave shielding effect, thus make the most of the microwave cannot incident into the metamaterial, so it cannot achieve effective loss. According to the above analysis, this unidirectional parallel arrangement has its advantages, that is, the absorption strength of the material can be dynamically tuned through the orientation of the CF. This bidirectional impedance variable material is expected to be used in smart and intelligent materials in the future, but it also has shortcomings in some applications, such as radar stealth materials that require broadband absorption, so the next section will improve this aspect.

### 3.3 Absorption performance of the metamaterials with orthogonal arrangement of CF and FSA ribbons

In order to realize that both orientations of the both orthogonal direction can improve the absorbing performance, present works make an improvement on the basis of the above work. Specifically, from the perspective of design, when the two orthogonal direction adopt CF arrangement, can get rid of the orientation of CF, but previous researchers have proved that orthogonal arranged CF would reduce the absorbing performance [1], it shows that CF in the perpendicular to the electric field is crucial in the performance of impedance, parallel to the electric field of the CF cannot play a role, therefore, this paper does not adopt orthogonal arrangement of CF itself, but introduces FSA ribbon to improve the absorbing performance. Specifically, CF and FSA ribbons are combined to form an orthogonal structure distributed in the matrix, as shown in Figure 5a. Under this kind of metastructure distribution, while in pure geometrical perspective is fourfold symmetrical, but the two orthogonal direction material is qualitative different, from the material point of view is still a double symmetric, therefore, there are still two orientation is different, need to test the CF is parallel to the electric field (FSA ribbon is perpendicular to the electric field) and perpendicular to the electric field (FSA ribbon

parallel to the electric field) wave absorption performance, as shown in Figures 5b and 5c. It can be seen from the figure that both orientations can improve the absorbing properties when the CF and FSA ribbons are combined to form a metastructural material. The sample with the best absorption performance is the CF with a spacing of 30 mm. The absorption bandwidth is 9.76–14.46 GHz and 9.96–14.1 GHz when the CF is parallel and perpendicular to the electric field, respectively, and corresponding absorption peak are respectively  $-16.17$  dB (12 GHz) and  $-13.89$  dB (11.88 GHz). Although the effective absorption bandwidth is lower when perpendicular to the electric field than when parallel to the electric field, it is still larger than that of the pure matrix material. Moreover, the absorption performance optimum spacing is 30 mm, which is larger than the optimal spacing (20 mm) of best reflection loss in metamaterial with only CF distribution. This phenomenon indicates the orthogonal metastructure in order to reduce the density of unit cells to achieve the optimal effect, also shows that optimum microwave absorption performance has certain metastructure unit cells distribution density range. Microwaves can be incident on metamaterial at different angles, and this angle change will also cause the change of absorption properties. It can be reasonably concluded that metamaterials with carbon fiber and bands can achieve excellent absorption performance at different angles, because the existence of their metastructure can scatter electromagnetic waves and dissipate electromagnetic energy. At the same time, the metastructure has periodicity at any angle, which can cause the electromagnetic field to produce phase difference and loss.

Furthermore, in order to clarify the mechanism of the coupling effect of CF and FSA ribbon to enhance the absorbing property, the electromagnetic field of the material is simulated and calculated in this paper, as shown in Figure 6. When the CF is parallel to the electric field, as shown in Figure 6a, the upper CF strengthens the electric field, while the lower CF weakens the electric field. As mentioned above, this situation makes the phase difference of the reflected electric field of the material and cause microwave loss, and the FSA ribbon can also have strong resonance with the electric field. Under this orientation arrangement, the magnetic field is weakened in both the CF and FSA ribbons (Fig. 6a), indicating that the

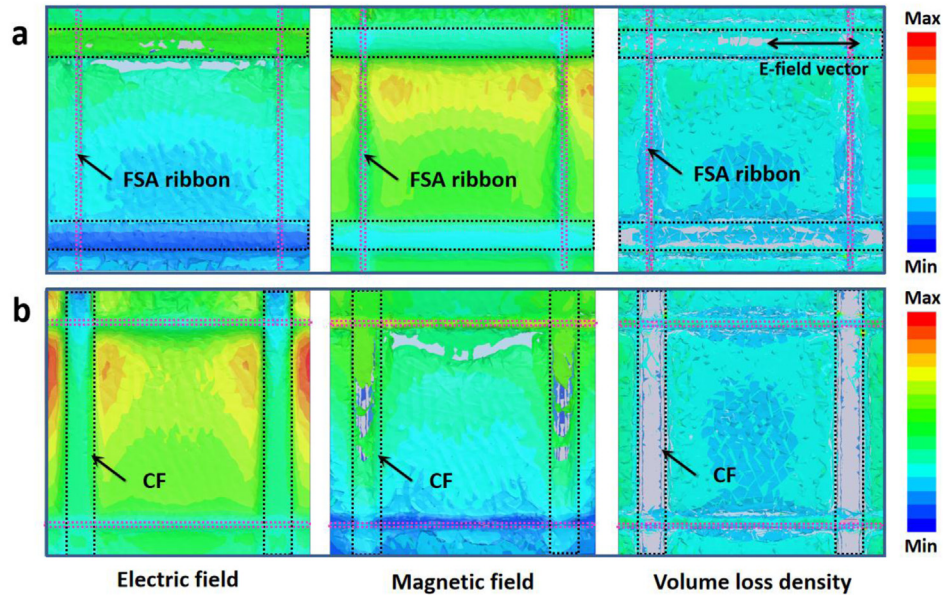


**Fig. 6.** Electric field, magnetic field and loss density distributions of sample with orthogonal distributed of CF and FSA ribbon, when the CF (a) Parallel to the electric field and (b) Perpendicular to the electric field.

**Table 1.** Typical microwave absorption metamaterials.

Materials	Thickness (mm)	Structures	Absorption bandwidth [GHz] (RL $\leq$ -10 dB)	References
ITO/PET/PMMA	3.85	Windmill	8–18	[27]
ITO	5.5	Square ring	5.5–19.7, 22.5–27.5	[29]
ITO	5	Bowtie	5.8–12.2	[39]
Carbon black	17	Square	2.35–18	[25]
Carbon	About 12	pyramidal	2–18	[28]
Al <sub>2</sub> O <sub>3</sub>	1.7	Square	About 11–12	[40]
HEA	20	chiral	4–18	[34]
CIP/PU & FSA ribbons, CF	1	Orthogonal structure	9.76–14.46	Present work

Comments: ITO, indium tin oxide; HEA, high entropy alloys, PET, polyethylene glycol terephthalate; PMMA, polymethyl methacrylate.

microwave loss is mainly due to the magnetic loss, which is also proved by the loss density in Figure 6a, since the distribution of the loss density is consistent with the electric field distribution. When the CF is perpendicular to the electric field, the electric field is weakened at both the CF and FSA ribbons (Fig. 6b), indicating that the electric loss is weakened.

However, the magnetic losses appear to be enhanced because of the enhanced magnetic field at the CF perpendicular to electric field. Especially, the FSA alloy ribbon has a loss effect. The upper ribbon enhances the magnetic field, while the lower ribbon weakens the magnetic field (Fig. 6b), which can cause phase difference in the magnetic field and loss of microwave. The loss density shown in Figure 6b is also concentrated in the FSA ribbons. The simulation results show that, although there is no attenuation of the CF, the loss enhancement of the FSA ribbon makes up for the poor absorbing performance caused by the CF perpendicular to the electric field. Additionally, the loss effect of CF and FSA ribbons stem

from the dielectric and magnetic loss (Fig. 2), which exhibit the intrinsic parameter of materials generated by electric dipoles relaxation and nature resonance and thus work in the metastructures. Table 1 exhibits the superiority in comparison with other reported microwave absorption metamaterials. Table 1 shows that most of the microwave absorption metamaterials prepared in previous studies are very thick because it is difficult for thin layer microwave absorbing metamaterials to obtain broadband absorption. The study in this paper provided a basis for the study of thin layer metamaterials.

## 4 Conclusions

In conclusion, thin-layer microwave absorbing metamaterials are prepared by combining the metastructure with the absorbing matrix. CF and FSA ribbons are distributed in the middle of two layers of CIP/PU resin matrix to form a sandwich structure, and the CF and FSA ribbons are

arranged into a metastructure. When only the CF are arranged into the matrix, the effective absorption bandwidth increases from 9.4–13.44 GHz to 11–16.8 GHz compared with the pure matrix when the CF are parallel to the electric field vector and the distance between adjacent CF is 20 nm. The absorption mechanism of CF with different orientations was clarified by equating the metastructure of CF to capacitance and inductance. Furthermore, the CF and FSA ribbons are arranged in the matrix in an orthogonal form, the best absorbing performance occurs when the spacing is 30 nm. The effective absorption bandwidth is 9.76–14.46 GHz when the CF is parallel to the electric field, and 9.96–14.1 GHz when the CF is perpendicular to electric field. The simulation results show that both CF and FSA ribbons can produce phase difference in electromagnetic field through resonance, and FSA ribbon can produce loss increase when CF has no loss, so as to make-up for the poor absorbing performance caused by CF perpendicular to the electric field. Through the research approach of this paper, we demonstrated a robust, high-yield, scalable, and low-cost fabrication of applied thin-layer microwave absorption metamaterials.

The authors acknowledge the Supported by Program for the National Natural Science Foundation of China (No. 52103334, 52071053, U1704253), China Postdoctoral Science Foundation (2020M680946, 2020M670748), the Fundamental Research Funds for the Central Universities (DUT20GF111), and the Fundamental Research Funds of Shaanxi Key Laboratory of Artificially-Structured Functional Materials and Devices (AFMD-KFJJ-211102).

## References

1. A. Shah et al., Enhanced microwave absorption by arrayed carbon fibers and gradient dispersion of Fe nanoparticles in epoxy resin composites, *Carbon* **96**, 987 (2016)
2. A. Shah et al., Microwave absorption and flexural properties of Fe nanoparticle/carbon fiber/epoxy resin composite plates, *Compos. Struct.* **131**, 1132 (2015)
3. L. Huang et al., Bioinspired metamaterials: multibands electromagnetic wave adaptability and hydrophobic characteristics, *Small* **15**, 1902730 (2019)
4. Q. Yuchang et al., Graphene nanosheets/BaTiO<sub>3</sub> ceramics as highly efficient electromagnetic interference shielding materials in the X-band, *J. Mater. Chem. C* **4**, 371 (2016)
5. L. Huang et al., Novel broadband electromagnetic-wave absorption metasurfaces composed of C-doped FeCoNiSiAl high-entropy-alloy ribbons with hierarchical nanostructures, *Compos. Part B: Eng.* **244**, 110182 (2022)
6. H. Pang et al., Research advances in composition, structure and mechanisms of microwave absorbing materials, *Compos. Part B: Eng.* **224**, 109173 (2021)
7. Z. Zhang et al., A review on metal-organic framework-derived porous carbon-based novel microwave absorption materials, *Nano-Micro Lett.* **13**, 56 (2021)
8. H. Zhao et al., Biomass-derived porous carbon-based nanostructures for microwave absorption, *Nano-Micro Lett.* **11**, 24 (2019)
9. C. Zhang et al., Structure engineering of graphene nanocages toward high-performance microwave absorption applications, *Adv. Opt. Mater.* **10**, 2101904 (2021)
10. X.-J. Zhang et al., Enhanced microwave absorption property of reduced graphene oxide (RGO)-MnFe<sub>2</sub>O<sub>4</sub> nanocomposites and polyvinylidene fluoride, *ACS Appl. Mater. Interfaces* **6**, 7471 (2014)
11. M. Cao et al., Thermally driven transport and relaxation switching self-powered electromagnetic energy conversion, *Small* **14**, 1800987 (2018)
12. H. Sun et al., Cross-stacking aligned carbon-nanotube films to tune microwave absorption frequencies and increase absorption intensities, *Adv. Mater.* **26**, 8120 (2014)
13. Y. Gao et al., Improved microwave absorbing property provided by the filler's alternating lamellar distribution of carbon nanotube/carbonyl iron/poly (vinyl chloride) composites, *Compos. Sci. Technol.* **158**, 175 (2018)
14. L. Huang et al., Chiral asymmetric polarizations generated by bioinspired helical carbon fibers to induce broadband microwave absorption and multispectral photonic manipulation, *Adv. Opt. Mater.* **10**, 2200249 (2022)
15. L. Song et al., Assembled Ag-doped  $\alpha$ -MnO<sub>2</sub>@ $\delta$ -MnO<sub>2</sub> nanocomposites with minimum lattice mismatch for broadband microwave absorption, *Compos. Part B: Eng.* **199**, 108318 (2020)
16. Y. Qing et al., Evolution of double magnetic resonance behavior and electromagnetic properties of flake carbonyl iron and multi-walled carbon nanotubes filled epoxy-silicone, *J. Alloys Compd.* **583**, 471 (2014)
17. K.S. Sista et al., Carbonyl iron powders as absorption material for microwave interference shielding: a review, *J. Alloys Compd.* **853**, 157251 (2021)
18. Z. Jia et al., Laminated microwave absorbers of A-site cation deficiency perovskite La<sub>0.8</sub>FeO<sub>3</sub> doped at hybrid RGO carbon, *Compos. Part B: Eng.* **176**, 107246 (2019)
19. L. Huang et al., Ultra-flexible composite metamaterials with enhanced and tunable microwave absorption performance, *Compos. Struct.* **229**, 111469 (2019)
20. Y. Li et al., Quinary high-entropy-alloy@graphite nanocapsules with tunable interfacial impedance matching for optimizing microwave absorption, *Small* **18**, 2270016 (2022)
21. J. Ding et al., Boosted interfacial polarization from multishell TiO<sub>2</sub>@Fe<sub>3</sub>O<sub>4</sub>@PPy heterojunction for enhanced microwave absorption, *Small* **15**, 1902885 (2019)
22. Z. Zou et al., 0D/1D/2D architectural Co@C/MXene composite for boosting microwave attenuation performance in 2–18 GHz, *Carbon* **193**, 182 (2022)
23. P. Liu et al., Hollow engineering to Co@N-doped carbon nanocages via synergistic protecting-etching strategy for ultrahigh microwave absorption, *Adv. Funct. Mater.* **31**, 2102812 (2021)
24. W.-L. Song et al., Constructing repairable meta-structures of ultra-broad-band electromagnetic absorption from three-dimensional printed patterned shells, *ACS Appl. Mater. Interfaces* **9**, 43179 (2017)
25. M. Li et al., A broadband compatible multispectral metamaterial absorber for visible, near-infrared, and microwave bands, *Adv. Opt. Mater.* **6**, 1701238 (2018)
26. T. Kim et al., Hierarchical metamaterials for multispectral camouflage of infrared and microwaves, *Adv. Functional Mater.* **29**, 1807319 (2019)

27. C. Zhang et al., Broadband metamaterial for optical transparency and microwave absorption, *Appl. Phys. Lett.* **110**, 143511 (2017)
28. K.-L. Zhang et al., Weather-manipulated smart broadband electromagnetic metamaterials, *ACS Appl. Mater. Interfaces* **10**, 40815 (2018)
29. D. Hu et al., Optically transparent broadband microwave absorption metamaterial by standing-up closed-ring resonators, *Adv. Opt. Mater.* **5**, 1700109 (2017)
30. W. Li et al., Broadband radar cross section reduction by in-plane integration of scattering metasurfaces and magnetic absorbing materials, *Res. Phys.* **12**, 1964 (2019)
31. F. Ding et al., Ultra-broadband microwave metamaterial absorber, *Appl. Phys. Lett.* **100**, 103506 (2012)
32. L. Huang et al., Broadband microwave absorption and adaptable multifunctionality of carbonaceous chiral metamaterials under deep subwavelength thickness, *ACS Appl. Electr. Mater.* (2021)
33. L. Huang et al., Bionic composite metamaterials for harvesting of microwave and integration of multifunctionality, *Compos. Sci. Technol.* **204**, 108640 (2021)
34. L. Huang et al., Bioinspired gyrotropic metamaterials with multifarious wave adaptability and multifunctionality, *Adv. Opt. Mater.* **8**, 2000012 (2020)
35. K.N. Rozanov, Ultimate thickness to bandwidth ratio of radar absorbers, *IEEE Trans. Antennas Propagat.* **48**, 1230 (2000)
36. M. Ning et al., Dumbbell-Like Fe<sub>3</sub>O<sub>4</sub>@N-doped carbon@2H/1T-MoS<sub>2</sub> with tailored magnetic and dielectric loss for efficient microwave absorbing, *ACS Appl. Mater. Interfaces* (2021)
37. Z. Zhang et al., Synthesizing CN<sub>x</sub> heterostructures on ferromagnetic nanoparticles for improving microwave absorption property, *Appl. Surf. Sci.* **564**, 150480 (2021)
38. Q. Li et al., Toward the application of high frequency electromagnetic wave absorption by carbon nanostructures, *Adv. Sci.* **6**, 1801057 (2019)
39. T. Jang et al., Transparent and flexible polarization-independent microwave broadband absorber, *ACS Photonics* **1**, 279 (2014)
40. Y. Li et al., Refractory metamaterial microwave absorber with strong absorption insensitive to temperature, *Adv. Opt. Mater.* **6**, 1800691 (2018)

**Cite this article as:** Lingxi Huang, Yuping Duan, Huifang Pang, Thin layers of microwave absorbing metamaterials with carbon fibers and FeSi alloy ribbons to enhance the absorption properties, *EPJ Appl. Metamat.* **10**, 3 (2023)